Investigation on velocity vector estimation by crossed-shape probe

Tatsuya Yano, Hiromu Fujisawa, Masaaki Omura, Ryo Nagaoka, and Hideyuki Hasegawa† (Univ. Toyama)

1. Introduction

The non-invasive dynamical measurement of the carotid artery wall by ultrasound is used for early diagnosis of atherosclerosis. In our previous study, the paper showed that the out-of-plane displacement (slice, *y* axis) component affects long-axis (*x*-*z*) plane estimation[1]. To estimate the out-of-plane displacement component, the crossed-shape probe is proposed. The array layout of the crossed-shape probe was designed with 2 sub arrays that intersected the main array. The 2 sub arrays estimate wall displacement in the short-axis cross-section. The purpose is to quantify the reliability of the long-axis estimation by referring to the *y*-axis displacement.

In this study, numerical simulation was implemented in the conditions of the proposed crossed-shape probe, and the accuracy of the estimated velocity vector was evaluated.

2. Methods

2.1 Crossed-shape probe

In this study, the probe shown in **Fig.1** was used to simultaneously estimate the velocity vectors in the *x*, *y*, and *z* axis. The interval between subarrays was set at the minimum distance that is physically feasible, i.e., 7.8 mm.

2.2 Transmit sequence

The vector Doppler method was implemented in the repeated transmit sequence. The transmission was performed only in the main array. In transmission, non-steered beams focused on a depth of 20 mm were generated by 32 elements. The center of Tx positions was set at 0.4 mm intervals from -5.8 mm to +5.8 mm when the center position of the main array was 0 mm. The Tx positions were set in 2 consecutive transmissions at the same position. Therefore, the transmission of 1 packet consists of 60 Txs.

2.3 Receive beamforming

DAS beamforming was applied to the RF complex signal obtained by each transmit-receive event.

DAS beamforming in the main array was performed as described in the paper of vector Doppler with plane wave imaging[2]. The receiving steering angle was set to ±25 degrees. In long-axis imaging, 40 receive lines were constructed and the intervals in the lateral (*x*-axis) and depth (*z*-axis) directions were set to 0.2 mm and 0.02 mm, respectively.

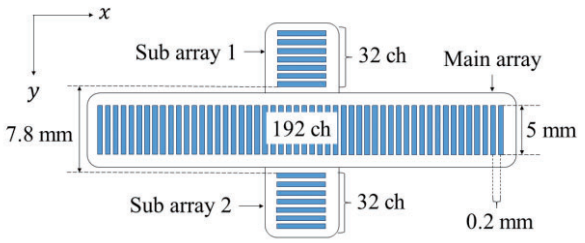

Fig 1. Illustration of the crossed-shape probe.

In short-axis imaging, The Han apodization was set at a fixed position in each sub array. Therefore, the receiving angle decreases as the depth of the focal position increases. 41 receive lines were constructed and the intervals in the slice (*y*-axis) and depth (*z*-axis) directions were set to 0.1 mm and 0.02 mm, respectively. In the beamforming for the subarray, the *x*-axis distance was included in the backward propagation distance because scattered waves are propagated in 3D. Therefore, the return propagation distance rr was defined as

$$rr = \sqrt{\left(x_p + x_{offset}\right)^2 + y_p^2 + z_p^2}, \qquad (1)$$

where $x_p, y_p,$ and z_p denote x, y, and z-axis positions of a point of interest, respectively. The x_{offset} for the x position was defined as

$$x_{offset} = \begin{cases} 0.5 \times E_{height} & (x_p < 0.5 \times E_{height}), \\ -0.5 \times E_{height} & (x_p > 0.5 \times E_{height}), \\ 0 & (\text{else}), \end{cases} \qquad (2)$$

where E_{height} was height of element.

2.4 Estimation of velocity vectors

The axial velocity can be estimated from the Doppler frequency shift of backscattered signals, which is expressed as

$$f_d = \frac{2v}{c} f_0 \cos\theta, \qquad (3)$$

where v, f_0, f_d, θ, and c are the tissue movement velocity, the center frequency of the ultrasound, the Doppler frequency shift of backscattered signals, the angle between tissue motion and axial direction, and the sound speed, respectively. Eq. (3) was modified

†hasegawa@eng.u-toyama.ac.jp

by defining the axial velocity as $u = (f_d/f_0) \times c$ and extended to 3D vector as

$$2|\boldsymbol{e}||\boldsymbol{v}| \cos\theta = u, \quad (4)$$

where $\boldsymbol{v} = [v_x\ v_y\ v_z]$ and $\boldsymbol{e}$ are 3D tissue movement velocity and a unit vector in the Tx/Rx axial direction, respectively. Eq. (4) is obtained from the dot product of vector $|\boldsymbol{e}||\boldsymbol{v}| \cos\theta = \boldsymbol{e} \cdot \boldsymbol{v}$ as

$$2\boldsymbol{e} \cdot \boldsymbol{v} = u, \quad (5)$$

$$2\boldsymbol{e} = \boldsymbol{e_t} + \boldsymbol{e_r}, \quad (6)$$

where $\boldsymbol{e_t}$ and $\boldsymbol{e_r}$ are unit vectors in the Tx and Rx axial directions, respectively. The unit vectors were calculated by referring to the point of interest position (x_p, y_p, z_p), Tx position (x_t, y_t, z_t), and Rx position(x_r, y_r, z_r), as illustrated in **Fig. 2(a)**.

The axial velocity was obtained by estimating the Doppler shift frequency f_d. In the long-axis, 2 axial velocities were estimated for the Rx angle θ_1 and θ_2. On other hand, in the short-axis, 2 axial velocities were estimated for the apertures of sub array 1 α_1 and sub array 2 α_2. Therefore, the 4 axial velocities and direction vectors were obtained for each point of interest in the long-axis cross section (y = 0 mm), as illustrated in **Fig. 2(b)**. The relationship expressed by Eq. (5) is valid for each angle and apodization, and expressed in a matrix form:

$$\boldsymbol{Av} = \boldsymbol{u} \Rightarrow$$

$$\begin{bmatrix} 2\boldsymbol{e}(x_p, z_p, \theta_1) \\ 2\boldsymbol{e}(x_p, z_p, \theta_2) \\ 2\boldsymbol{e}(y_p, z_p, \alpha_1) \\ 2\boldsymbol{e}(y_p, z_p, \alpha_2) \end{bmatrix} \begin{bmatrix} v_x \\ v_y \\ v_z \end{bmatrix} = \begin{bmatrix} u(x_p, z_p, \theta_1) \\ u(x_p, z_p, \theta_2) \\ u(y_p, z_p, \alpha_1) \\ u(y_p, z_p, \alpha_2) \end{bmatrix}. \quad (7)$$

The velocity vector $\boldsymbol{v}$ is estimated by the least-square method as

$$\boldsymbol{v} = (\boldsymbol{A}^T\boldsymbol{A})^{-1}\boldsymbol{A}^T\boldsymbol{u},$$

where $(\boldsymbol{A}^T\boldsymbol{A})^{-1}\boldsymbol{A}^T$ is the pseudoinverse of $\boldsymbol{A}$.

2.5 Simulation

In the present study, the diastolic motion of a carotid artery wall during an increase of internal pressure in blood vessels was simulated by an in-silico cylindrical tube phantom. The velocities in the long-axis cross section assigned to the phantom (true velocities) in x, y, and z axes are shown in **Figs. 3(T-*x*)-(T-*z*)**. **Figs. 3(T-*x*)** and **(T-*y*)** showing that the uniform velocities in x and y axis directions simulated the motion of a carotid artery being pulled by the heart. **Fig. 3(T-*z*)** shows that z-axis direction velocity, which were inversely proportional to the distance from the lumen. z-axis direction velocity simulated the dilation of the carotid artery due to an internal pressure increment induced by the contraction of a heart. Therefore, the anterior wall was moving in the upward direction, and the posterior wall was moving in the downward direction.

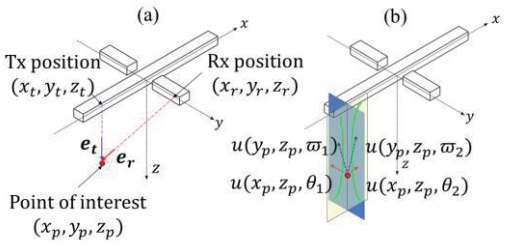

Fig. 2 Illustration of (a) Tx/Rx unit vectors (b) 4 axial velocities at point of interest.

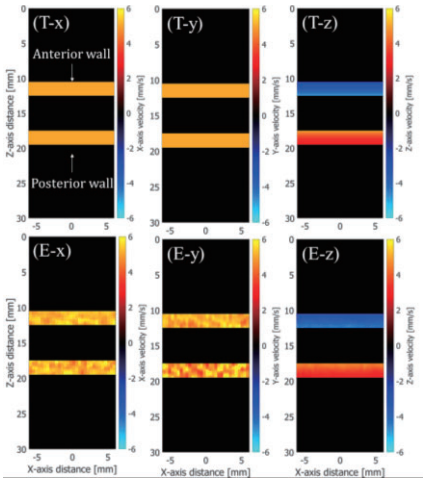

Fig. 3 True velocities set in the simulation (T-x)-(T-z) and the estimated velocities (E-x)-(E-z).

In this study, Field II ultrasound simulation program was used[3,4].

3. Results and Conclusion

Figs. 3(E-*x*)-(E-*z*) show that estimated velocities of each axial direction almost agree with the true one which was shown in Fig 3(T-x)-(T-z).

As **Fig. 3(E-*y*)** shows, the spatial variation in y axis velocities in the posterior wall was large. Since the short-axis (y-z) velocity estimation was received by a fixed aperture, the receiving angle became smaller at a deeper position. Therefore, y-axis velocity components were small, and the spatial variation might be large. In our future work, the effect of temporal averaging on the stability of the spatial velocity distribution will be investigated in a basic experiment.

References

1) T. Yano, M. Mozumi, M. Omura, R. Nagaoka, and H. Hasegawa., Jpn. J. Appl. Phys. **61**, SG1053-1-12 (2022).
2) H. Hasegawa, M. Omura, and R. Nagaoka., IEEE UFFC, **69**, 1301 - 1311 (2022).
3) J. A. Jensen, Med. Biol. Eng. Comput. **34**(1), 351-353, 1996
4) J. A Jensen and N. B. Svendsen, IEEE Trans. Ultrason. Ferroelectr. Freq. Control **39**, 262-267, 1992.